PHYSICAL REVIEW B **81**, 245420 (2010)

Symmetry-induced band-gap opening in graphene superlattices

Rocco Martinazzo*
Department of Physical Chemistry and Electrochemistry and CIMAINA, University of Milan, V. Golgi 19, 20133 Milan, Italy

Simone Casolo
Department of Physical Chemistry and Electrochemistry, University of Milan, V. Golgi 19, 20133 Milan, Italy

Gian Franco Tantardini
Department of Physical Chemistry and Electrochemistry and CIMAINA, University of Milan, V. Golgi 19, 20133 Milan, Italy and ISTM Institute for Molecular Science and Technology, V. Golgi 19, 20133 Milan, Italy

(Received 8 February 2010; revised manuscript received 12 April 2010; published 16 June 2010)

We study $n \times n$ honeycomb superlattices of defects in graphene. The considered defects are missing p_z orbitals and can be realized by either introducing C atom vacancies or chemically binding simple atomic species at the given sites. Using symmetry arguments and electronic-structure calculations we show that it is possible to open a band gap without breaking graphene point symmetry. This has the advantage that new Dirac cones appear right close to the gapped region. We find that the induced gaps have an approximate square-root dependence on the defect concentration $x=1/n^2$ and compare favorably with those found in nanoribbons at the same length scale.

DOI: 10.1103/PhysRevB.81.245420 PACS number(s): 73.20.Hb, 73.21.Cd, 81.05.U−, 73.20.At

I. INTRODUCTION

The recent isolation of graphene,[1] the one atom-thick layer of carbon atoms arranged in a honeycomb lattice, has triggered a wealth of studies in both fundamental and applied science. Graphene is a zero-gap semiconductor in which the valence and the conduction bands touch at the two inequivalent corners of the hexagonal Brillouin zone (BZ) (the so-called Dirac points). Its low-energy excitations experience a linear-energy dispersion and thus mimic the behavior of relativistic massless fermions.[2–5] This gives rise to a number of interesting phenomena such as an anomalous quantum Hall effect[2,3] and quasirelativistic Klein tunneling.[6] From a practical point of view, its unconventional properties with ballistic transport on a micrometer scale[7] and with carrier mobilities up to 2×10^5 $cm^2\ V^{-1}\ s^{-1}$ (Ref. 8) offer the possibility of high-performance interconnects in a hypothetical carbon-based nanoelectronics. However, since conductivity cannot be turned completely off, pristine graphene cannot be used as a transistor in logic applications, where high on/off ratios are required.[9,10] Field-switching capabilities depend on the presence and size of a band gap in the electronic structure.

Within the realm of single-layer graphene physics, electron confinement (such that occurring when rolling up graphene into single-walled nanotubes or cutting its edges to form nanoribbons) is the most effective way to open a gap in the band structure. In this case one partially breaks translational symmetry and let the two Dirac points hybridize, thereby opening a gap whose size is inversely proportional to the confinement length. This possibility has already been exploited and promising carbon nanotube/nanoribbon field-effect transistors realized.[9] Alternatively, one can break the point symmetry by rendering inequivalent the two sublattices of which graphene is made, thus turning the massless excitations into massive (relativistic) pseudoparticles.[11] This could be the source of the gap observed in a recent angle-resolved photoemission study of epitaxial graphene on a SiC substrate,[12,13] though different explanations are possible.[14,15]

In this work we explore a different possibility made available by recent progresses in patterning graphene with lithographic techniques.[16–19] Specifically, we study $n \times n$ honeycomb superlattices of defects on graphene (defined to be periodic structures of defects arranged to form a honeycomb-lattice commensurate with the substrate) and use symmetry arguments to design semiconducting structures. The considered defects are missing p_z orbitals and can be realized by either introducing C atom vacancies or chemically binding simple atomic species at the given sites. Differently from previous investigations of patterned graphene (see, e.g., Refs. 20 and 21 and the closely related study in Ref. 22), we show that a gap can be opened in this way *without* breaking graphene point symmetry. This implies that degeneracy may still occur in the valence (conduction) bands at the high-symmetry points in k space and, in that case, a k-linear structure close to these points is expected, i.e., new Dirac cones can be anticipated. These are similar to some extent to what has been theoretically suggested[23–27] and experimentally found[28] in a different kind of superlattices, namely, those obtained by subjecting graphene to an external periodic potential.

We estimate that the gap size in the proposed structures has an approximate inverse proportionality to the (super)lattice constant n and use tight-binding (TB) and *first-principles* calculations to validate these predictions. We show that new chiral, Dirac fermions are generated right close to the band edges and that their velocity depends linearly on $1/n$. The computed gaps are sizable and compare favorably with those found in nanoribbons at the same length scale,[29] thereby suggesting that the proposed structures have good field-switching capabilities. In addition, the preserved pseudorelativistic behavior of the charge carriers for energies beyond the gap may be important for all-carbon nanodevices working in the coherent-transport regime. In the case of similar graphene p-n junctions, for instance, intriguing phenomena

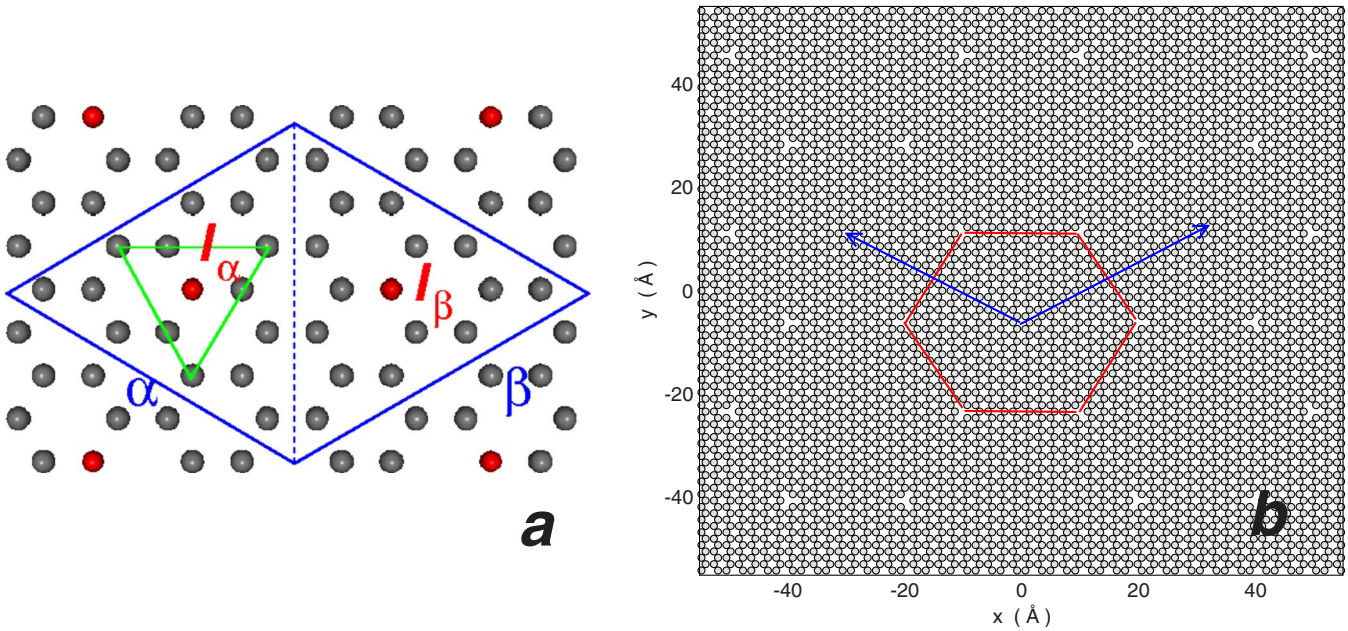

FIG. 1. (Color online) (a) The simplest symmetrically defective superlattice for $n=4$ [the (4,0) honeycomb]. Also indicated the two halves of the cell (α,β), their centers I_α, I_β (red balls) and one of the triangles $\Delta_{i,\alpha}$. A defect is a missing p_z orbital at I_α, I_β. (b) The (14,0) honeycomb along with the superlattice vectors (blue arrows) and its Wigner-Seitz supercell (red lines).

such as electron focusing have already been suggested.[30]

The paper is organized as follows. In Sec. II we present our symmetry arguments and derive some general rules to open a gap in the considered superlattices. In Sec. III we estimate its value and in Sec. IV we present the results of numerical calculations.

II. SYMMETRY AND BIPARTITISM

Graphene's unconventional electronic properties are strictly related to its D_{6h} point symmetry. The k group at the $K(K')$ high-symmetry points (D_{3h}) allows for doubly degenerate irreducible representations, and Bloch functions built with p_z orbitals of A and B sublattices span one of its two-dimensional irreducible representations (irreps), namely, E''. This is enough for the π-π^* degeneracy at the $K(K')$ point and for the unusual linear-dispersion relation, irrespective of the level of approximation.[31] These properties are captured by the simple TB model Hamiltonian

$$H = -t\sum_{\langle i,j\rangle} a_i^\dagger b_j + \text{H.c.} - t'\sum_{\langle\langle i,j\rangle\rangle} a_i^\dagger a_j - t'\sum_{\langle\langle i,j\rangle\rangle} b_i^\dagger b_j, \quad (1)$$

where $a_i^\dagger(b_i^\dagger)$ is the creation operator for an electron on site i of the A (B) sublattice, the first two sums run over nearest-neighboring sites in the honeycomb lattice and the second ones run over sites which are nearest neighbors in the triangular sublattices. The hopping t has been estimated to be ~ 2.7 eV whereas $t' \ll t$ has different values depending on the parametrization. When $t'=0$ the Hamiltonian describes a bipartite system, and we assume that this approximately holds for graphene. The consequences of relaxing this approximation will be addressed numerically in Sec. IV.

Bipartitism has a large impact on the electronic structure *via* the induced electron-hole (e-h) symmetry. For instance, it has long been known that in bipartite systems, at half filling, sublattice imbalances due to vacancies strongly affect the energy spectrum at the Fermi level through the introduction of midgap states.[32] According to theory[33,34] and experiment,[35] in graphene such states have a semilocalized nature with a $1/r$ dependence on the distance from the defect. By introducing an equal number of defects on each sublattice one restores balance, eliminates midgap states and a gap possibly opens. In general, however, there is no guarantee that the gap opens at K and does not close somewhere else in the BZ. Therefore, we focus here on $n\times n$ honeycomb patterns of defects only, in such a way to constrain (by symmetry) the changes in the band structure and possibly reduce accidental degeneracies. (One further possibility, namely, the $n\sqrt{3}\times n\sqrt{3}R30°$ superlattices, will be briefly considered later in this paper). In these structures the high-symmetry points where degeneracy is expected are Γ and K points, that is where the k groups (D_{6h} and D_{3h}, respectively) allow for doubly degenerate irreps. In the following we use $E(A)$ for a generic two-(one-) dimensional irreducible representation and denote as K_n, the K point of the $n\times n$ superlattice BZ. For a strictly bipartite system at half filling, degeneracy at the Fermi level occurs when the number of E irreps is odd; when this number is even degeneracy, if occurs, can be considered as accidental. Therefore, introducing symmetric defects in such a way to have an even number of E irreps *both* at Γ and K points a gap generally opens.

To show that this is indeed possible, we consider a generic $n\times n$ supercell and count the number of A and E irreps generated by the carbon atoms in cell (the so-called atomic representations). To this end, it is sufficient to consider that half of the cell which has D_{3h} symmetry with respect to its center I [see Fig. 1, panel (a)], the remaining half behaving simi-

TABLE I. Number of irreducible one-(A) and two-(E) dimensional representations (per cell) generated by the full atomic basis in a $n\times n$ honeycomb superlattice at Γ and K points of the corresponding BZ. In the table entries $m=[n/3]$.

Γ	A	E
$\bar{0}_3$	$6m^2$	$6m^2$
$\bar{1}_3$	$2(3m^2+2m+1)$	$2(3m^2+2m)$
$\bar{2}_3$	$2(3m^2+4m+2)$	$2(3m^2+4m+1)$
K_n	A	E
$\bar{0}_3$	$6m^2$	$6m^2$
$\bar{1}_3$	$2m(3m+2)$	$2m(3m+2)+1$
$\bar{2}_3$	$2(3m^2+4m+1)$	$2(3m^2+4m+1)+1$

larly. These two half cells (α and β in the following) play the role of A and B types of sites in the honeycomb superlattice. In each of them, the set of C atoms may be grouped in classes of equilateral triangles $\Delta_{i,\alpha}(\Delta_{i,\beta})$, plus a possible atom at $I_\alpha(I_\beta)$ as it happens when $n=3m+1$ and $n=3m+2$ (m integer). Each triangle spans $A+E$ irreps of the D_{3h} group (centered at I) which behave as s and (p_x,p_y) orbitals centered at I; the atom at I, when present, spans of course an A irrep. Then, by considering Bloch functions built with these s- and (p_x,p_y)-like orbitals it is possible to count the number of A and E irreps for each case.[36] At Γ the Bloch functions built with s-like orbitals centered on I_α and I_β span two A representations, whereas p_x,p_y-like functions span two E irreps; at K_n the first generate an E irrep whereas the latter span $2A+E$. These are also the irreps generated by the p_z orbitals of the C atoms as long as we discriminate between A and E types only. The overall result is given in Table I where the symbol $\bar{n}_3=\bar{0}_3,\bar{1}_3,\bar{2}_3$ identifies the three (congruence) classes modulo 3, i.e., the sequences $n=3m$, $3m+1$, and $3m+2$, respectively.

It follows from Table I that with the full atomic set (i.e., considering pure graphene) degeneracy occurs at the K_n points when either $n\in\bar{1}_3$ or $n\in\bar{2}_3$. This is consistent with the folding $K(K')\rightarrow K_n(K_n')$ and $K(K')\rightarrow K_n'(K_n)$, respectively. In the case $n\in\bar{0}_3$ both K and K' folds to Γ and therefore a fourfold degeneracy occurs; this can be considered accidental in this context as it cannot be predicted by the number of E irreps only. More interestingly, two important results concerning the introduction of p_z vacancies are easily proved.

(I) *By removing a* $\Delta_{i,\alpha}$, $\Delta_{i,\beta}$ pair only is not generally possible to open a gap. Here, $2(A+E)$ irreps are removed both at Γ and K_n, and no modification occurs on the parity of the E sets. Exceptions to this rule are, of course, those cases where degeneracy is accidental (as pure graphene in the $\bar{0}_3$ case which does show a gap after removal of one such pairs, see below).

(II) *When* $n\in\bar{1}_3$ or $n\in\bar{2}_3$ removal of the atoms at I_α and I_β does open a gap. In these cases, the atomic basis spans $2A$ at Γ and E at K_n, thereby turning the number of E irreps to be even at *both* special points. Also in this case, exceptions of residual accidental degeneracy are possible.

The second result provides a very simple way for opening a gap in two thirds of the cases, that is by introducing p_z vacancies at I_α and I_β. In practice, as already said in the introduction, this can be realized by either removing substrate atoms or using them to covalently bind simple adsorbates such as H atoms.[37] In the latter case, indeed, the C atoms involved in the chemisorption process turn their hybridization to sp^3 and effectively get out of the π-π^* band system. In the case of a C vacancy, on the other hand, there are three additional unpaired electrons per vacancy coming from the sp^2 network. The corresponding sp^2 dangling orbitals span $A+E$ in the local point group and would give rise to a Jahn-Teller distortion that breaks the symmetry of the superlattice (see, e.g., Ref. 38). In this case, then, we assume that dangling bonds are saturated, e.g., by exposing the substrate to a (low-energy) H-atom beam after creation of vacancies.

In this paper we mainly focus on the simplest defective superlattices, i.e., those with vacancies at I_α and I_β *only* and call them $(n,0)$ honeycombs. In general, the pair of integers $(n,p)[p=0,\ldots,\mathrm{int}(n^2/3)]$ can be used to identify a $n\times n$ honeycomb superlattice with $2p$ equilateral triangles symmetrically removed from the unit supercell, in addition to the atoms at their centers I_α and I_β when $n\in\bar{1}_3\cup\bar{2}_3$. Figure 1 shows two examples, (4,0) and (14,0) honeycombs.

Before closing this section, it is worth comparing the above results with those that can be analogously found in $n\sqrt{3}\times n\sqrt{3}R30°$ superlattices, as the latter have been employed in defining graphene antidot lattices[39,40] and similar structures have been experimentally realized.[18,19] From the symmetry point of view such superlattices behave as the $\bar{0}_3$ case above in that both K and K' always fold to Γ. This means that they are generally semiconducting, i.e., a band gap opens whenever the fourfold degeneracy in the folded graphene band structure (accidental in this context) is removed by symmetrically introducing a number of vacancies. In other words, in $n\sqrt{3}\times n\sqrt{3}R30°$ superlattices symmetry always guarantees a gap for a sufficiently defective substrate.

III. BAND-GAP ESTIMATE

From the point of view of the low-energy carrier dynamics, the atomic-scale defects we are considering in this work break the pseudospin conservation and, introducing intervalley-scattering and backscattering mechanisms, suppress Klein tunneling.[6] As they are also periodically arranged hybridization occurs and opens a gap in the band structure. By dimensional analysis, the gap size should scale as v_F/l_n, where v_F is the Fermi velocity in pristine graphene ($v_F=\sqrt{3}at/2$ with Hamiltonian (1), $a=\sqrt{3}d_{\mathrm{C\text{-}C}}\approx 2.46$ Å being its lattice constant and $d_{\mathrm{C\text{-}C}}$ the C-C bond length) and l_n is the distance between defects ($l_n=na/\sqrt{3}$).

To estimate the size of the induced gap at the K_n point of our $(n,0)$ honeycombs we perform a lattice renormalization[41] by making use of the bipartite nature of the Hamiltonian $H=H_{AB}+H_{BA}$. This simplifies the problem by

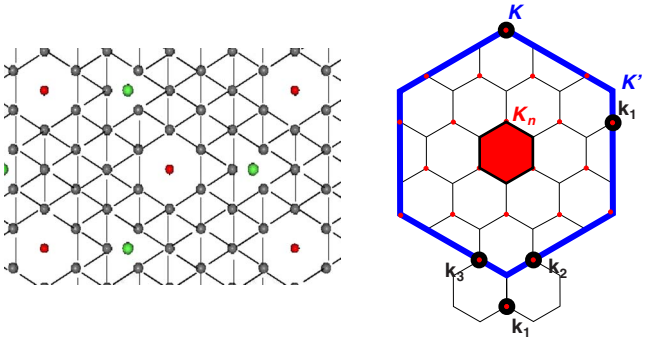

FIG. 2. (Color online) Left panel: the renormalized triangular lattice corresponding to the (4,0) honeycomb (grey balls). Red and green balls mark the positions of A and B defects. Right panel: Brillouin zones for graphene (blue borders) and for the structure shown on the left panel (red). Also indicated the four lowest-energy $\mathbf{k}$ points (K and $\mathbf{k}_i$ $i=1-3$) for the calculation in the text (black circles).

halving the state space of interest. Indeed, since H only allows transitions from the A to the B subspaces (H_{BA}) and *vice versa* (H_{AB}) it is sufficient to consider the problem in the A space only with Hamiltonian[42] $\tilde{H}_{AA}=H_{AB}H_{BA}$. For any nonzero eigenvalue $\tilde{\epsilon}_i$ and eigenvector $|\psi_{A,i}\rangle$ of this Hamiltonian there exist two solutions of the original problem with eigenvalues $\epsilon_i=\pm\sqrt{\tilde{\epsilon}_i}$ and eigenvectors $|\psi_{A,i}\rangle\pm|\psi_{B,i}\rangle$, where $|\psi_{B,i}\rangle$ is defined to be $|\psi_{B,i}\rangle=\tilde{\epsilon}_i^{-1/2}H_{BA}|\psi_{A,i}\rangle$; if $\tilde{\epsilon}_i=0$, $|\psi_{A,i}\rangle$ is already a H eigenvector. The converse is also true, namely, from any eigenvector $|\psi_i\rangle$ the two projections $|\psi_{A,i}\rangle$ and $|\psi_{B,i}\rangle$ onto A and B supspaces satisfy $H_{BA}|\psi_{A,i}\rangle=\epsilon_i|\psi_{B,i}\rangle$ and $\tilde{H}_{AA}|\psi_{A,i}\rangle=\epsilon_i^2|\psi_{A,i}\rangle$; that is, in studying $\tilde{H}_{AA}$ one only misses possible zero eigenstates in the B subspace.[43]

In graphene the renormalized Hamiltonian $\tilde{H}_{AA}$ describes a triangular lattice with on-site energy t^2Z [where t is the hopping term of Eq. (1) and $Z=3$ is the coordination number of A atoms in the original honeycomb lattice] and hopping t^2 between neighbors in the triangular lattice. Defects are of two kinds: while A vacancies translate simply into A vacancies in the renormalized lattice, B vacancies modify both the coordination number and the hopping between A sites. The renormalized $(n,0)$ honeycomb for $n=4$ is shown in the left panel of Fig. 2 whereas the right panel of the same figure displays the superlattice Brillouin zone along with that of graphene (BZ). The state space at K_n is given by its n^2 replicas within BZ and comprises K or K' depending on whether $n\in\bar{1}_3$ or $n\in\bar{2}_3$. Quasidegenerate perturbation theory is necessary to estimate the ground-state energy $\tilde{\epsilon}_0(K_n)$ (and hence the gap $\epsilon_{gap}=2\sqrt{\tilde{\epsilon}_0}$), but it becomes intractable at large n (i.e., at very small defect concentration $x=1/n^2$) because a huge number of K_n replicas gets close to K and K' points. Therefore, we consider x sufficiently small that the defects are isolated from each other, but large enough that a few-state calculation is reliable. The smallest set of K_n replicas contains K and the $\mathbf{k}_i$ vectors ($i=1-3$) shown in Fig. 2 (right panel) for the case $n=4$ and corresponds to the set of (graphene) Bloch functions $|\psi_0\rangle=|\psi_K\rangle$ and $|\psi_i\rangle=|\psi_{\mathbf{k}_i}\rangle$ built with p_z orbitals at A sites; the case $n\in\bar{2}_3$ is analogous except that K is replaced with K'. $|\psi_0\rangle$ spans the A_2'' irrep of the k group at K_n (D_{3h}) whereas $\{|\psi_i\rangle\}$ spans $A_2''+E''$. Thus it is possible to setup a two-dimensional problem in the A_2'' subspace. The corresponding Hamiltonian matrix can be obtained from the $\tilde{H}_{AA}$ matrix elements between (graphene) Bloch states, Eq. (2)

$$\langle\psi_{\mathbf{k}'}|\tilde{H}_{AA}|\psi_{\mathbf{k}}\rangle = t^2\delta_{\mathbf{k}',\mathbf{k}}[3+F(\mathbf{k})] - xt^2\delta_{\mathbf{k}',\mathbf{k}+\mathbf{g}}\{e^{i\mathbf{g}\boldsymbol{\delta}_A}[3+F(\mathbf{k}')+F(\mathbf{k})]+e^{i\mathbf{g}\boldsymbol{\delta}_B}f(\mathbf{k}')^*f(\mathbf{k})\}. \quad (2)$$

Here $F(\mathbf{k})=\Sigma_{i=1}^{6}e^{-i\mathbf{k}\boldsymbol{\delta}_i'}$, $f(\mathbf{k})=\Sigma_{i=1}^{3}e^{-i\mathbf{k}\boldsymbol{\delta}_i}$ (where $\boldsymbol{\delta}_i'$ and $\boldsymbol{\delta}_i$ are the vectors joining AA and AB nearest neighbors, respectively), $\mathbf{g}$ is a reciprocal superlattice vector and $\boldsymbol{\delta}_A$ and $\boldsymbol{\delta}_B$ are the position vectors of the defects in the unit supercell. In deriving Eq. (2) periodicity of the superlattice has been used and the defects have been considered as isolated ($n>2$). With the help of Eq. (2) and of the symmetry properties of $F(\mathbf{k})$ and $f(\mathbf{k})$, the Hamiltonian matrix in the above A_2'' space reads as

$$t^2\begin{bmatrix} 3x & -x\sqrt{3}F_x \\ -x\sqrt{3}F_x & 3+F_x-9x(2+F_x)\end{bmatrix}, \quad (3)$$

where $F_x=F(\mathbf{k}_1)\sim -3+3(2\pi/3)^2x-\sqrt{3}(2\pi/3)^3x^{3/2}$. The lowest eigenvalue $\tilde{\epsilon}_0[\sim 3xt^2(0.561-0.961\sqrt{x})]$ of this matrix allows us to estimate the energy gap $\epsilon_{gap}=2\sqrt{\tilde{\epsilon}_0}$ at the K_n point. This function is plotted in Fig. 3(a) along with the results of tight-binding calculations to be discussed in the next section.

IV. CALCULATIONS

We performed a number of tight-binding calculations by numerically diagonalizing the tight-binding Hamiltonian (1) with periodic boundary conditions. In addition, we investigated a smaller number of superlattices by means of periodic density-functional theory (DFT) as implemented in the Vienna *ab initio* simulation package suite.[45,46] The generalized gradient approximation, as provided by the Perdew-Burke-Ernzerhof[47] functional, and the projector-augmented wave method within the frozen-core approximation[48] were used throughout. Details are analogous to those reported in a recent work[37] and will not be repeated here. We only note that a $6\times6\times1$ Γ-centered k-points mesh that included all the special points of the Brillouin zone (i.e., where the minimum gap was expected) was used and that extensive tests were performed to check convergence on the computed band gaps.

The results of tight-binding calculations are reported in Fig. 3. The numerically computed gaps decrease slightly faster than $\sqrt{x}$ with a best-fit exponent ~ 0.66. Clearly, the estimate given in Sec. II deteriorates at small x where a larger number of states would be needed, but it behaves rather well for moderate values of x. Tight-binding calculations reveal that the minimum gaps occur either at M or Γ [see Fig. 3(b)], depending on x and on the sequence considered, but behave similarly to the gaps at K_n. Differences between the two sequences appear at large x and reflect the different shape of the low-energy bands (not shown). A best fit of $\epsilon_{gap}/t=c_1x^{\alpha}(1+c_2x^{\beta})$ to the numerical results, also reported in Fig. 3(a), gives $(c_1,c_2,\alpha,\beta)=(3.34,-4.99,$

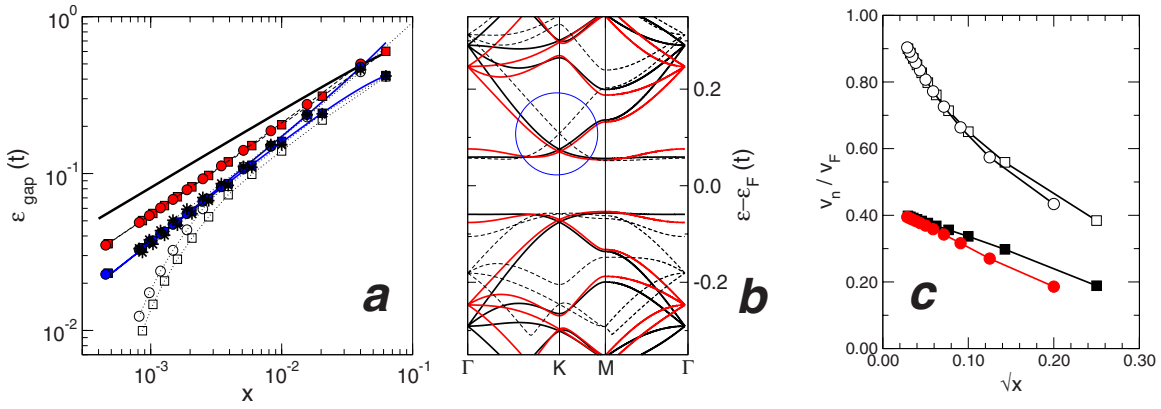

FIG. 3. (Color online) (a) Energy gaps (in units of t) for the $(n,0)$ honeycombs as functions of $x=1/n^2$, squares for $n\in\bar{1}_3$ and circles for $n\in\bar{2}_3$. Filled symbols are results of tight-binding calculations with $t'=0$ (red for the gap at K_n, blue for the full gap) and the bold black line represents the K_n gap estimate given in Sec. III. Open symbols are full gap results for $|t'|=0.1t$ and stars are for TB calculations including the third-neighbor hoppings, using the parameters of Ref. 44. (b) Low-energy band structures of the (13,0) (black) and (14,0) (red) honeycombs as obtained from tight-binding calculations with $t'=0$. Dashed lines for the (14,0) structure when $t'=0.1t$. (c) Group velocity (in units of Fermi velocity in pristine graphene) at the new Dirac point [circle in panel (b)] as a function of $\sqrt{x}$ for the $\bar{1}_3$ (squares) and $\bar{2}_3$(circles) sequences (filled and open symbols for $t'=0t$ and $t'=0.1t$, respectively).

$0.65,1.14)$ for $n\in\bar{1}_3$ and $(3.37,+2.9,0.66,0.88)$ for $n\in\bar{2}_3$.

A closer inspection to the band structure [see Fig. 3(b)] shows, as expected, that degeneracy occurs at K_n and Γ points for selected energies and gives rise to a k-linear-energy dispersion. The interesting point is that new Dirac cones are created right close to the band edge,[49] thereby suggesting that they readily act as conducting channels once the gate-controlled Fermi level exceeds the quasi-dispersionless bands at the gap edge(s). The group velocity at these new Dirac points is closely related to the size of the gap and scales like $\sqrt{x}$, as can be guessed from a higher order analysis and seen in Fig. 3(c) from the numerics. Though smaller than v_F such velocity is sizable enough $(0.2-0.4v_F)$ to represent a good compromise for the pseudorelativistic behavior of the carriers in graphene if a band gap has to be introduced.

The limit $x\to 0$ deserves some comment as it is clear from Fig. 3(c) that the low-energy band structure of our honeycombs is qualitatively different from that of graphene even in such limit. The origin of this oddity lies in the combined action of spatial and e-h symmetry or, in other words, this behavior is a further manifestation of the deep impact that vacancies have on graphene electronic structure. The limit $x\to 0$ represents the ideal, perfectly "compensated" situation (i.e., with no sublattice imbalance) in which defects are almost isolated from each other and yet periodically arranged, in such a way that they always hybridize and open a gap in the band structure (by symmetry). This means that no midgap states and accompanying local magnetic moments would arise in such situation. This contrasts with the case of randomly distributed defects, where midgap states appear at low concentrations even in absence of imbalance fluctuations (see the perfectly compensated case in Fig. 9 of Ref. 34) as a consequence of a semilocal imbalance created in the neighborhood of each defect. Then, the physically meaningful limit would be restored by any kind of imperfections in the superlattice and/or, as we show below, by the introduction of the next-to-nearest-neighbor interactions which break the e-h symmetry. Notice, however, that the behavior for $x\to 0$ of the density of states (DOS) close to the Fermi energy can be reconciled *on average* with that of pristine graphene, see Fig. 4.

Returning to the main goal of the present paper we now show that the symmetry arguments of Sec. II are robust against e-h symmetry breaking, at least for reasonably small t'/large x. To this end, we performed tight-binding calculations including hopping beyond the nearest-neighbor one. As can be seen in Fig. 3(a), introduction of the next-to-nearest-neighbors interaction t', though differently for the two sequences considered, only affects the results at small x. For these values of x valence and conduction bands start to overlap at some point x_c because of the asymmetry introduced in the energy spectrum. This asymmetry "disconnects" the two

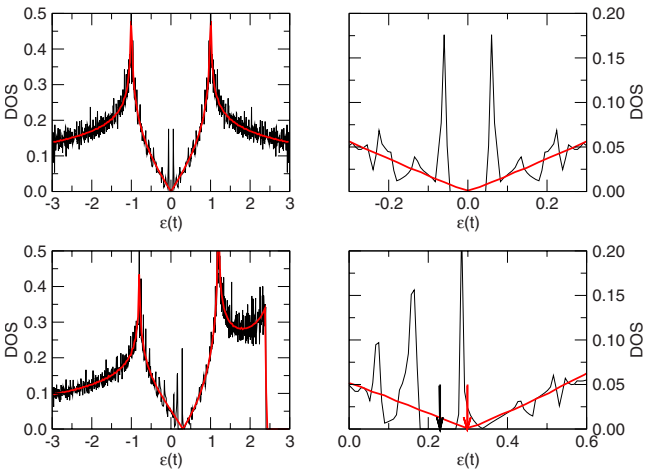

FIG. 4. (Color online) Normalized, tight-binding density of states in the (14,0) honeycomb (black lines) and in graphene (red). Top and bottom panels for $t'=0t$ and $t'=0.1t$, respectively. The arrows in the lower right panel mark the positions of the Fermi levels. Energy in units of t.

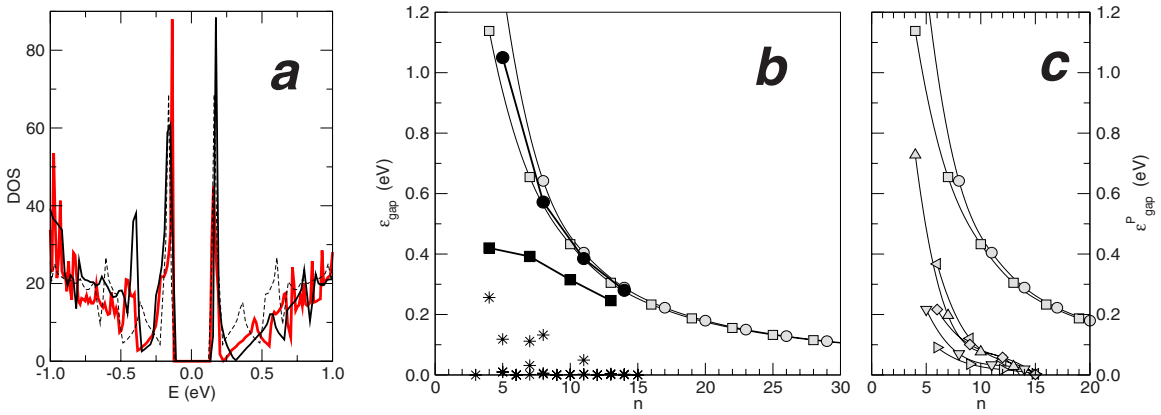

FIG. 5. (Color online) (a) Low-energy density of states in the (14,0) honeycomb as computed at the DFT (red) and TB level (same results as in Fig. 4 with black solid line for $t'=0.1t$ and dashed line for $t'=0$). (b) DFT results for the energy gap in $(n,0)$ honeycombs as functions of n (filled symbols). For comparison, also reported are the tight-binding results of Fig. 3 (open symbols) with $t=2.7$ eV and $t'=0$. Squares for $n \in \bar{1}_3$, circles for $n \in \bar{2}_3$. Stars are energy gaps in a number of superlattices with an asymmetric AB pair of defects per cell. (c) TB results (normalized to the number P of pairs of defects, $\epsilon^P_{gap}=\epsilon_{gap}/P$) for some of the (n,p) honeycombs described in the text: triangles for $p=1$, diamonds for $p=2$. Squares and circles as in (b).

new Dirac cones above and below the Fermi level, and one of them (the one above the Fermi level for $t'/t>0$) reduces to the Dirac cone in pristine graphene when $x \to 0$, as can be seen from the computed group velocity in Fig. 3(c) (see also Fig. 4 for the behavior of the DOS at low energies). The position of the critical value x_c shifts to larger x when increasing t' but remains small for realistic values [for $t'=0.1t$ used in Fig. 3(a) $x_c<10^{-3}$]. Addition of the third-neighbor hopping t'', which has been found[44] to be comparable to t', does not modify the overall result, as this interaction does not contribute to the breaking of the e-h symmetry. This is shown in Fig. 3(a) where the results obtained using the *first-principles*-derived tight-binding parameters of Ref. 44 are almost indistinguishable from the case $t'=0$ in the range of x considered, since in this case $|t'| \sim 0.06t$.

To further investigate the effect of breaking the e-h symmetry and, more importantly, to address the role of electron correlation we performed gradient-corrected DFT calculations on a number of $(n,0)$ honeycombs made by adsorbed H atoms. Adsorption of hydrogen atoms on graphene was studied at the same DFT level in a previous work,[37] where we investigated the effects of graphene electronic structure on this process. Calculations reported here are an example of how adsorption of chemical species affects graphene electronic structure and may be used for material design. The results of DFT calculations for our honeycombs structures are reported in Fig. 5(b) up to $n=14 (x \sim 0.005)$; for larger values of n DFT calculations become prohibitive. As can be seen from Fig. 5(b) DFT results show a reduced gap size with respect to TB ones in all the cases considered but the effect is much more pronounced in the $\bar{1}_3$ sequence than in the $\bar{2}_3$ one. In particular, DFT results for $n=5$, 8, 11, 14 closely parallel the TB ones (t has been set to its accepted value, $t=2.7$ eV), despite the fact that the first refer to a realistic situation where defects are H atoms while in TB calculations defects are modeled by simple p_z vacancies. A closer inspection to the density of states [shown in Fig. 5(a) for $n=14$] reveals that in these cases TB calculations require a nonzero t' to better reproduce the DFT-computed DOS, but they correctly predict the size of the gap even when $t'=0$. [Figure 3(b) shows the corresponding TB band structures for $n=14$. Notice in Fig. 5(a) the linear behavior of the DOS at $E \gtrsim 0.1$ eV which corresponds to the Dirac point marked in Fig. 3(b).] Discrepancies in the $\bar{1}_3$ sequence at small n needs further investigation, though they are in line with the introduction of the next-to-nearest-neighbor hopping [Fig. 3(a)]. Similar behavior was found for the gap in armchair graphene nanoribbons where it was explained by the modified nearest-neighbor hoppings for the sites close to the defect.[29] In any case, both the size of the gap and its dependence on n are promising for future applications.

Finally, to underline the role played by symmetry in designing the defective structures, TB results for different superlattices are also reported in Fig. 5. In Fig. 5(b) we show the gap obtained when an asymmetric pair of defects (of type AB) is periodically arranged in the same $n \times n$ superlattices (star symbols); in Fig. 5(c) we report the results of different symmetric structures with a variable number of triangles of vacancies, i.e., (n,p) honeycombs with $p>0$ (including the sequence $\bar{0}_3$). Notice that results of Fig. 5(c) have been normalized to the number of pairs of defects to emphasize that the $(n,0)$ honeycombs considered in this paper show the largest gaps with the minimum number of defects per supercell.

In practice, it may be experimentally challenging to realize the atomic-scale patterned structures discussed so far. It is, however, feasible[16–19] to produce superlattices of circular holes with diameters as small as 2–3 nm and periodicity ~ 5 nm, i.e., structures similar to those suggested by Pedersen *et al.*[39,40] Therefore, we have also considered honeycomb antidot superlattices obtained by creating holes of radius R_h at the centers I_α and I_β of each half cell. As unstable structures may form in this way, we only made sure that each C atom had a coordination number greater than one. In Fig. 6 we report the TB energy gaps for different hole radii as func-

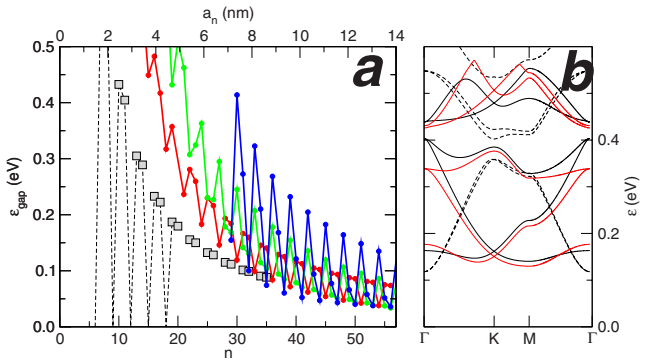

FIG. 6. (Color online) (a) Energy gaps in honeycomb antidot superlattices as functions of the superlattice constant a_n. From left to right, solid curves for hole diameters $2R_h$ of 1, 2, and 4 nm. Dashed line is for the case $R_h < d_{C\text{-}C}$, which reduces to the $(n,0)$ honeycombs of the main text for $n \in \bar{1}_3 \cup \bar{2}_3$ (square symbols) and to pristine graphene otherwise. (b) Band structure (for $E>0$ only) of the antidot superlattices $n=21$ (dashed lines) and $n=22$, 23 (solid black and red lines, respectively) for $2R_h=1$ nm.

tions of the superlattice constants $(a_n=na)$. The results fit well to a R_h/a_n^2 scaling law suggested for similar antidot superlattices,[39] which reduces to $1/a_n$ for R_h small. As a matter of fact, for $R_h < d_{C\text{-}C}$ the above antidot lattices reduce to our $(n,0)$ honeycombs for $n \in \bar{1}_3$ or $n \in \bar{2}_3$ and to pristine graphene otherwise. This explains the oscillating behavior of the gap as a function of the superlattice constant, a feature which persists for larger R_h as a consequence of the different folding properties of three sequences above. In Fig. 6(b) we also report the band structure for three different antidot superlattices with a hole diameter 1 nm long to show that low-energy Dirac cones can be found in this case, too. This differs from what happens in the previously suggested triangular superlattices of holes (see, e.g., Fürst *et al.*[50] for a review), which do not show such Dirac cones. It is worth noticing, however, that if the same triangular superlattices are created by subjecting graphene to an external periodic potential new Dirac cones do appear at the M points of the corresponding BZ.[23]

V. SUMMARY AND CONCLUSIONS

To summarize, we have studied graphene superlattices of defects where a gap at the Fermi level opens because of the preserved symmetry. This differs from conventional ways of introducing a gap in the band structure by symmetry breaking, in that it partially preserves the pseudorelativistic behavior of the carriers. With the help of tight-binding and density-functional-theory calculations we have shown that the induced gap is indeed sizable and, furthermore, that new Dirac cones are formed right close to the gap edge(s). All this suggests that novel field-effect transistors might be obtained by patterning graphene to form such superstructures. Though the simple atomic-scaled structures discussed at length in this paper may seem challenging at present, the related honeycomb antidot superlattices should be experimentally feasible. Actually, in a recent work Bai *et al.*[51] have reported a graphene nanomesh closely related to the proposed structures.

*rocco.martinazzo@unimi.it

[1] K. S. Novoselov, A. K. Geim, S. V. Morozov, D. Jiang, Y. Zhang, S. V. Dubonos, I. V. Gregorieva, and A. A. Firsov, Science **306**, 666 (2004).
[2] K. S. Novoselov, A. K. Geim, S. V. Morozov, D. Jiang, M. I. Katsnelson, I. V. Gregorieva, S. V. Dubonos, and A. A. Firsov, Nature (London) **438**, 197 (2005).
[3] Y. Zhang, Y.-W. Tan, H. L. Stormer, and P. Kim, Nature (London) **438**, 201 (2005).
[4] A. K. Geim and K. S. Novoselov, Nature Mater. **6**, 183 (2007).
[5] A. H. Castro Neto, F. Guinea, N. M. R. Peres, K. S. Novoselov, and A. K. Geim, Rev. Mod. Phys. **81**, 109 (2009).
[6] M. I. Katsnelson, K. S. Novoselov, and A. K. Geim, Nat. Phys. **2**, 620 (2006).
[7] F. Schedin, A. K. Geim, S. V. Morozov, E. W. Hill, P. Blake, M. I. Katsnelson, and K. S. Novoselov, Nature Mater. **6**, 652 (2007).
[8] K. Bolotin, K. Sikes, Z. Jiang, M. Klima, G. Fudenberg, J. Hone, P. Kim, and H. L. Stormer, Solid State Commun. **146**, 351 (2008).
[9] P. Avouris, Z. Chen, and V. Perbeinos, Nat. Nanotechnol. **2**, 605 (2007).
[10] K. Novoselov, Nature Mater. **6**, 720 (2007).
[11] G. W. Semenoff, Phys. Rev. Lett. **53**, 2449 (1984).
[12] S. Y. Zhou, G.-H. Gweon, A. V. Fedorov, P. N. First, W. A. de Heer, D.-H. Lee, F. Guinea, A. H. Castro Neto, and A. Lanzara, Nature Mater. **6**, 770 (2007).
[13] S. Y. Zhou, G.-H. Gweon, A. V. Fedorov, P. N. First, W. A. de Heer, D.-H. Lee, F. Guinea, A. H. Castro Neto, and A. Lanzara, Nature Mater. **7**, 259 (2008).
[14] A. Bostwick, T. Ohta, T. Seyller, K. Horn, and E. Rotenberg, Nat. Phys. **3**, 36 (2007).
[15] E. Rotenberg, A. Bostwick, T. Ohta, J. L. McChesney, T. Seyller, and K. Horn, Nature Mater. **7**, 258 (2008).
[16] J. C. Meyer, C. O. Girit, M. F. Crommie, and A. Zettl, Appl. Phys. Lett. **92**, 123110 (2008).
[17] M. D. Fischbein and M. Drndic, Appl. Phys. Lett. **93**, 113107 (2008).
[18] T. Shen, Y. Q. Wu, M. A. Capano, L. P. Rokhinson, L. W. Engel, and P. D. Ye, Appl. Phys. Lett. **93**, 122102 (2008).
[19] J. Eroms and D. Weiss, New J. Phys. **11**, 095021 (2009).
[20] R. N. Costa Filho, G. A. Farias, and F. M. Peeters, Phys. Rev. B **76**, 193409 (2007).
[21] B. Gharekhanlou, M. Alavi, and S. Khorasani, Semicond. Sci. Technol. **23**, 075026 (2008).
[22] R. P. Tiwari and D. Stroud, Phys. Rev. B **79**, 205435 (2009).
[23] C.-H. Park, L. Yang, Y.-W. Son, M. L. Cohen, and S. G. Louie, Phys. Rev. Lett. **101**, 126804 (2008).
[24] C.-H. Park, L. Yang, Y.-W. Son, M. L. Cohen, and S. G. Louie, Nat. Phys. **4**, 213 (2008).

[25] C.-H. Park, Y.-W. Son, L. Yang, M. L. Cohen, and S. G. Louie, Phys. Rev. Lett. **103**, 046808 (2009).
[26] L. Brey and H. A. Fertig, Phys. Rev. Lett. **103**, 046809 (2009).
[27] M. Barbier, P. Vasilopoulos, and F. M. Peeters, Phys. Rev. B **81**, 075438 (2010).
[28] I. Pletikosić, M. Kralj, P. Pervan, R. Brako, J. Coraux, A. T. N'Diaye, C. Busse, and T. Michely, Phys. Rev. Lett. **102**, 056808 (2009).
[29] Y. W. Son, M. L. Cohen, and S. G. Louie, Phys. Rev. Lett. **97**, 216803 (2006).
[30] V. V. Cheianov, V. Fal'ko, and B. L. Altshuler, Science **315**, 1252 (2007).
[31] J. C. Slonczewski and P. R. Weiss, Phys. Rev. **109**, 272 (1958).
[32] M. Inui, S. A. Trugman, and E. Abrahams, Phys. Rev. B **49**, 3190 (1994).
[33] V. M. Pereira, F. Guinea, J. M. B. Lopes dos Santos, N. M. R. Peres, and A. H. Castro Neto, Phys. Rev. Lett. **96**, 036801 (2006).
[34] V. M. Pereira, J. M. B. Lopes dos Santos, and A. H. Castro Neto, Phys. Rev. B **77**, 115109 (2008).
[35] M. M. Ugeda, I. Brihuega, F. Guinea, and J. M. Gómez-Rodríguez, Phys. Rev. Lett. **104**, 096804 (2010).
[36] Those pairs of triangles which are not compatible with the hexagonal symmetry should be compound in hexagons. The final result, however, is unchanged.
[37] S. Casolo, O. M. Løvvik, R. Martinazzo, and G. F. Tantardini, J. Chem. Phys. **130**, 054704 (2009).
[38] P. O. Lehtinen, A. S. Foster, Y. Ma, A. V. Krasheninnikov, and R. M. Nieminen, Phys. Rev. Lett. **93**, 187202 (2004).
[39] T. G. Pedersen, C. Flindt, J. Pedersen, N. A. Mortensen, A.-P. Jauho, and K. Pedersen, Phys. Rev. Lett. **100**, 136804 (2008).
[40] T. G. Pedersen, C. Flindt, J. Pedersen, A.-P. Jauho, N. A. Mortensen, and K. Pedersen, Phys. Rev. B **77**, 245431 (2008).
[41] G. G. Naumis, Phys. Rev. B **76**, 153403 (2007).
[42] If H is the second quantization version of the Hamiltonian a projection onto the single-particle space is implied.
[43] Their presence can be detected by defining A to be the majority species and comparing the number of zero A eigenstates with the sublattices imbalance.
[44] B. R. K. Nanda and S. Satpathy, Phys. Rev. B **80**, 165430 (2009).
[45] G. Kresse and J. Hafner, Phys. Rev. B **47**, 558 (1993).
[46] G. Kresse and J. Furthmüller, Comput. Mater. Sci. **6**, 15 (1996).
[47] J. P. Perdew, K. Burke, and M. Ernzerhof, Phys. Rev. Lett. **77**, 3865 (1996).
[48] P. E. Blöchl, Phys. Rev. B **50**, 17953 (1994).
[49] For a single, doubly degenerate level a cone can only appear at the $K(K')$ point. At Γ (where the relavant k group has inversion symmetry) it is easy to show by $\mathbf{k}\cdot\mathbf{p}$ perturbation theory that degeneracy cannot be lifted at first order for parity reasons.
[50] J. A. Fürst, J. G. Pedersen, C. Flindt, N. A. Mortensen, M. Brandbyge, T. G. Pedersen, and A.-P. Jauho, New J. Phys. **11**, 095020 (2009).
[51] J. Bai, X. Zhong, S. Jiang, Y. Huang, and X. Duan, Nat. Nanotechnol. **5**, 190 (2010).